STRESS INTENSITY FACTOR K_I DETERMINATION, USING PHOTOELASTIC ANALYSIS AND NUMERICAL TECHNIQUE

Daniel Lelis de Almeida, dla.bh@uol.com.br
Perrin Smith Neto, psmith@pucminas.br
Pedro Américo Almeida Magalhães Júnior, pamerico@pucminas.br
Cristina Almeida Magalhães, crisamagalhaes@gmail.com
Pontifícia Universidade Católica de Minas Gerais, Av. Dom Jose Gaspar, 500, 30535-610, Belo Horizonte, Minas Gerais, Brazil.
Clovis Sperb de Barcellos, clovis.barcellos@gmail.com
Universidade Federal de Santa Catarina, Campus Reitor Joao David Ferreira Lima, 88040-970, Florianopolis, Santa Catarina, Brazil.
Marco Antonio Dutra Quinan, quinanm@cdtn.br
Centro de Desenvolvimento da Tecnologia Nuclear , Av. Antônio Carlos, 6627, 30161-970, Belo Horizonte, Minas Gerais, Brazil.

Abstract. *In this paper addresses the determination of stress intensity factor K_I using photoelastic experimental analysis and numerical technique by finite element method. A compact type (CT) specimen made by polycarbonate PSM-1 was submitted to pure tension and a simulation for testing Fracture Mechanics was also performed using Ansys® software. Results of both techniques are in agreement of about 3% on average. Methodology for obtaining stress intensity factor presented in this work allows application in developing prototypes for mechanical parts.*

Keywords*: Stress intensity factor, photoelastic, experimental analysis, finite element method, Fracture Mechanics and Ansys® software.*

1. INTRODUCTION

Analysis of structural components were increasedly applied with the rise of studies in areas of Fatigue, Fracture Mechanics, Structural Reliability and numerical methods. When structures or components have discontinuities such as cracks, stress fields existing at the tip of these cracks have singularities. Thus, in these cases, theory of elasticity is not sufficient to predict structural behavior of materials under the action of efforts, from the standpoint of determining the structure moment of collapse. A difficulty in making such prediction is due especially to geometry of the crack tip, which has a radius of curvature close to zero, generating local stresses that attempt to infinity. With these unique local stresses, both yield stress and failure stress of the material may be exceeded, even for small applied loads.

Fracture Mechanics models takes into account natural state of stress in crack tip (Irwin and De Wit, 1983), proposing the use of some parameters, including stress intensity factor K, which considers the loads applied to structure and geometry of the crack. Based on these factors, it is possible to take decisions about safety of the structure, comparing value of K with value of fracture toughness K_c of the material (Soares,1997).

Photoelasticity, technique discovered in the early twentieth century, has been used for stress analysis on components. It stands for the speed in obtaining results and didactic view of the distributions of stresses throughout the component, described by the fringe pattern (Dally and Riley, 2005). In particular, plays an important role in determining the stress intensity factors for specific configurations of geometry and loading (Soares,1997).

2. THEORETICAL ASPECTS

Dally and Riley (2005) present Method of Irwin, Method of Various Parameters for determination of K_I and Method of Overdeterministic. A data set, selected from the region near the crack tip, is used to calculate stress intensity factor using photoelastic technique.

2.1. Method of Irwin

Irwin proposed a relationship between stress intensity factor in opening loads, and characteristics of isochromatic fringes near the crack tip (Fig. 1).

Based on experimental observations, Irwin suggested a modification in the equations of Westergaard (Soares,1997) introducing of a constant stress σ_{0x}. Thus the stress field near the crack tip would be expressed by equations:

$$\sigma_{xx} = \frac{K_I}{\sqrt{2\pi r}} \cos\frac{\theta}{2}\left(1 - \sin\frac{\theta}{2}\sin\frac{3\theta}{2}\right) - \sigma_{0x} \quad (1)$$

$$\sigma_{yy} = \frac{K_I}{\sqrt{2\pi r}} \cos\frac{\theta}{2}\left(1 + \sin\frac{\theta}{2}\sin\frac{3\theta}{2}\right) - \sigma_{0x} \quad (2)$$

$$\tau_{xy} = \frac{K_I}{\sqrt{2\pi r}} sin\frac{\theta}{2} cos\frac{\theta}{2} cos\frac{3\theta}{2} \quad (3)$$

where: $\sigma_{0x} = \sigma_{yy}^{\infty} - \sigma_{xx}^{\infty}$, and σ_{yy}^{∞} is remote stress applied in the direction of axis *y* .σ_{xx}^{∞} is remote stress applied in the direction of axis *x*.

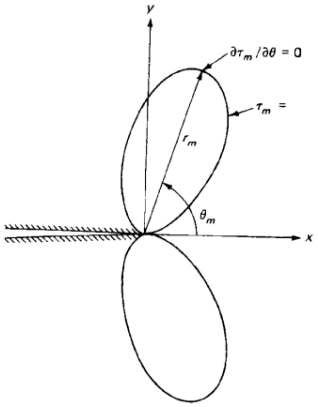

Figure 1. Geometrical characteristics of the isochromatic crack tip (Dally and Riley, 2005).

Maximum shear stress τ_m can be expressed as a function of stress components, as given by equation:

$$(2\tau_m)^2 = \left(\sigma_{yy} - \sigma_{xx}\right)^2 + \left(2\tau_{xy}\right)^2 \tag{4}$$

Therefore:

$$(2\tau_m)^2 = \frac{K_I^2}{2\pi r} sin^2\theta + \frac{2\sigma_{0x}K_I}{\sqrt{2\pi r}} sin\theta \times sin\frac{3\theta}{2} + \sigma_{0x}^2 \tag{5}$$

where *r* is the distance from a given point of isochromatic fringe to the origin of the coordinate system centerd at the notch tip and θ is the angle formed by the coordinate axes *x* and the straight line that connects a given point of the isochromatic and origin, in accordance with Fig. 1.

Observing the geometry of the isochromatic fringes, note that $\frac{\partial\tau_m}{\partial\theta} = 0$ at the extreme position on the fringe, where $r = r_m$ and $\theta = \theta_m$. Differentiating Eq. (5) with respect to θ and using $\frac{\partial\tau_m}{\partial\theta} = 0$, one obtains:

$$\sigma_{0x} = \frac{-K_I}{\sqrt{2\pi r_m}}\left[\frac{sin\theta_m cos\theta_m}{cos\theta_m sin\left(\frac{3\theta}{2}\right) + \frac{3}{2} sin\theta_m cos\left(\frac{3\theta}{2}\right)}\right] \tag{6}$$

Combining Eq. (5) with Eq. (6), results an expression for σ_{ox} ,

$$\sigma_{0x} = \frac{-2\tau_m cos\theta_m}{cos(3\theta_m/2\theta)\sqrt{cos^2\theta_m + 9sin^2\theta_m/4}} \tag{7}$$

Substitution of Eq. (7) into Eq. (5) leads to an expression for stress intensity factor, K_I:

$$K_I = \frac{2\tau_m\sqrt{2\pi r_m}}{sin\theta_m}\left[1 + \left(\frac{2}{3tan\theta_m}\right)^2\right]^{1/2}\left[1 + \frac{2tan(3\theta_m/2)}{3tan\theta_m}\right] \tag{8}$$

The term τ_m in Eq. (8) is determined by taking as basis data provided by isochromatic fringes since the maximum shear stress is given by:

$$\tau_m = \frac{Nf}{2h} \tag{9}$$

2.2. Methods of Various parameters for K_I determination

Using two methods of parameters, such as Irwin, it is necessary that the used data should be very close to the crack tip, in the limited region, for $r_m/a < 0.03$, in which Eq. (6) is valid. There are two difficulties associated with this restriction. The first is that the region $r/e < 0.5$ is under three-dimensional stress state and plane state assumptions

used in Eq. (6) and Eq. (8) are not valid. To avoid errors arising from this situation, inequality $0.03a > r_m > h/2$ must be satisfied. The concept of valid region for methods of two parameters is shown schematically in Fig. 2.

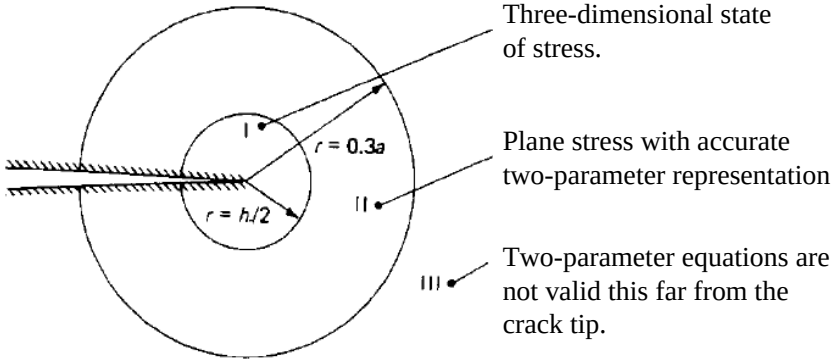

Figure 2. Concept of the three regions near the crack tip (Dally and Riley, 2005).

The second difficulty relates to the measurement position coordinates, r_i and θ_i, for each point on isochromatic fringes. Since the width of the fringe has imprecise definition, it is a source of significant errors. To overcome these difficulties, it was used a higher order representation and Eq. (6) was replaced by the following equation:

$$\sigma_{xx} = A_0 r^{-1/2} cos\frac{\theta}{2}\left(1 - sin\frac{\theta}{2}sin\frac{3\theta}{2}\right) + 2B_0 + A_1 r^{1/2} cos\frac{\theta}{2}\left(1 + sin^2\frac{\theta}{2}\right) + 2B_1 r\, cos\theta + A_2 r^{3/2}\left(cos\frac{3\theta}{2} - \frac{3}{2}sin\theta sin\frac{\theta}{2}\right) + 2B_2 r^2(sin^2\theta + cos2\theta)$$

$$\sigma_{yy} = A_0 r^{-1/2} cos\frac{\theta}{2}\left(1 + sin\frac{\theta}{2}sin\frac{3\theta}{2}\right) + A_1 r^{1/2} cos\frac{\theta}{2}\left(1 - sin^2\frac{\theta}{2}\right) + A_2 r^{3/2}\left(cos\frac{3\theta}{2} + \frac{3}{2}sin\theta sin\frac{\theta}{2}\right) + 2B_2 r^2 sin^2\theta$$

$$\tau_{xy} = A_0 r^{-1/2} cos\frac{\theta}{2} sin\frac{\theta}{2} cos\frac{3\theta}{2} - A_1 r^{1/2} sin\frac{\theta}{2} cos^2\frac{\theta}{2} - 2B_1 r\, sin\theta - 3A_2 r^{3/2} sin\frac{\theta}{2} cos^2\frac{\theta}{2} - 2B_2 r^2 sin\theta \quad (10)$$

The coefficients A_0, A_1, A_2, B_0, B_1 and B_2 are unnamed and must be determined. Stress intensity factor, K_I, can then be obtained based on values A_0 and σ_x, which in turn are obtained through B_0.

$$K_I = \sqrt{2\pi} A_0$$

$$\sigma_{0x} = -2B_0 \quad (11)$$

Other coefficients are included only for increasing the accuracy of K_I. Substituting Eq. (10) and Eq. (11) in Eq. (4), results:

$$\left(\frac{Nf}{2h}\right)^2 = \left(\frac{\sigma_{yy} - \sigma_{xx}}{2}\right)^2 + \left(\tau_{xy}\right)^2 = D^2 + T^2 \quad (12)$$

where:

$$D = \frac{\sigma_{yy} - \sigma_{xx}}{2} = \sum_{n=0}^{2}\left(n - \frac{1}{2}\right) A_n r^{n-1/2} sin\theta \times sin\left(n - \frac{3}{2}\right)\theta + \sum_{m=0}^{2} B_m r^m [m\, sin\theta \times sin(m\theta) + cos(m\theta)] \quad (13)$$

$$T = \tau_{xy} = -\sum_{n=0}^{2}\left(n - \frac{1}{2}\right) A_n r^{n-1/2} sin\theta \times sin\left(n - \frac{3}{2}\right)\theta - \sum_{m=0}^{2} B_m r^m [m\, sin\theta \times sin(m\theta) + cos(m\theta)] \quad (14)$$

2.3. Overdeterministic Method

Equation (12) is not linear and matrix methods associated with linear algebra cannot be applied. To solve it, iterative methods must be used to seek solution of the problem. One of these methods is the overdeterministic method proposed by Dally (Dally and Riley, 2005). The use of a large number of data (greater than the number of unknowns) leads to a set of relationships with overdeterministic in the form of Eq. (12). A solution based on the method of least squares is an alternative to solve this problem. The solution is obtained by defining a function g_k, based on Eq. (12):

$$g_k = D_k^2 + T_k^2 - \left(\frac{N_k f_\sigma}{2h}\right)^2 = 0 \quad (15)$$

where the subscript *k* indicates that $g_k$value is evaluated at point (r_k, θ_k) in isochromatic order N_k, located on zone II in Fig. 2. Since both D_k and T_k depend on A_n and B_m, when correct values of these constants are used in Eq. (15), value of g_k will be equal zero for all values of *K*. Iterative processes assign initial values to the coefficients. As these values are not correct, g_k will be nonzero. The correction process is done interactively expanding g_k in Taylor series, according to Eq. (16):

$$g_k^{i+1} = g_k^i + \frac{\partial g_k^i}{\partial A_0}\Delta A_0 + \frac{\partial g_k^i}{\partial A_1}\Delta A_1 + \cdots + \frac{\partial g_k^i}{\partial B_0}\Delta B_0 + \frac{\partial g_k^i}{\partial B_1}\Delta B_1 + \cdots \tag{16}$$

Since $g_k = 0$ (Eq. 15):

$$-g_k^i = \frac{\partial g_k^i}{\partial A_0}\Delta A_0 + \frac{\partial g_k^i}{\partial A_1}\Delta A_1 + \cdots + \frac{\partial g_k^i}{\partial B_0}\Delta B_0 + \frac{\partial g_k^i}{\partial B_1}\Delta B_1 + \cdots \tag{17}$$

In matrix form:

$$[g] = [c][\Delta] \tag{18}$$

where,

$$[g] = \begin{bmatrix} -g_1 \\ -g_2 \\ \vdots \\ -g_L \end{bmatrix},\ [\Delta] = \begin{bmatrix} \Delta A_0 \\ \vdots \\ \Delta A_N \\ \Delta B_0 \\ \vdots \\ \Delta B_M \end{bmatrix} \text{ and } [c] = \begin{bmatrix} \frac{\partial g_1}{\partial A_0} \cdots \frac{\partial g_1}{\partial A_N} \cdots \frac{\partial g_1}{\partial B_0} \cdots \frac{\partial g_1}{\partial B_M} \\ \vdots \\ \frac{\partial g_L}{\partial A_0} \cdots \frac{\partial g_L}{\partial A_N} \cdots \frac{\partial g_L}{\partial B_0} \cdots \frac{\partial g_L}{\partial B_M} \end{bmatrix} \tag{19}$$

L is the total number of sample points; *M* and *N* are the upper truncation of the series. It is usually enough to make *N = M = 2* to obtain a series with six terms with *L = 5 (N + M +2)* sampled points. Partial derivatives are obtained based on Eq. (20):

$$\frac{\partial g_k}{\partial A_n} = 2D_k \frac{\partial D_k}{\partial A_n} + 2T_k \frac{\partial T_k}{\partial A_n} \tag{20}$$

The system shown in Eq. (18) is solved by method of least squares, multiplying both sides of equation by transposed matrix $[c]$, resulting in Eq. (21).

$$[c]^T[g] = [c]^T[c][\Delta] \tag{21}$$

Setting $[a] = [c]^T[c]$:

$$[\Delta] = [a]^{-1}[c]^T[g] \tag{22}$$

Iterative process was used to obtain A_n and B_m coefficients, as follows:

1) Select points on isochromatic fringe patterns in zone II, with "*L*" significant points for representation of these fringes. Join for each L points, data set (r_k, θ_k, N_k).
2) Assume initial values for coefficients A_0, A_1, ..., A_N, ..., B_0, B_1, ..., B_M. The algorithm is not sensitive to initially adopted values.
3) Calculate elements of the matrices $[c]$ and $[g]$.
4) Solve Eq. (22) and correct estimates for the unknown constants, using Eq. (23):

$$\begin{aligned} A_0^{L+1} &= A_0^L + \Delta A_0 \\ &\vdots \\ A_N^{L+1} &= A_N^L + \Delta A_N \\ B_0^{L+1} &= B_0^L + \Delta B_0 \\ &\vdots \\ B_N^{L+1} &= B_N^L + \Delta B_N \end{aligned} \tag{23}$$

5) Repeat steps 3 and 4 until all increments ΔA_0, ..., ΔB_M become sufficiently small. Convergence is rapid and usually reach good results with less than 10 iterations.
6) K_I is determined using Eq. (11).

3. EXPERIMENTAL ANALYSIS

In photoelasticity, the determination of more accurate results depends on several factors, including choice of material. For this reason, it was chosen to build a specimen polycarbonate material made of PSM-1 material, certified, seeking thereby to improve reliability of the test in order to determine stress intensity factor. Size and specimen used in trials can be seen in Figures 3 and 4.

The specimen was tested in a circular polariscope manufactured by Measurements Group®. It was applied a load of 300N and 50N to 50N stages of the images were captured (Figures 5-11).

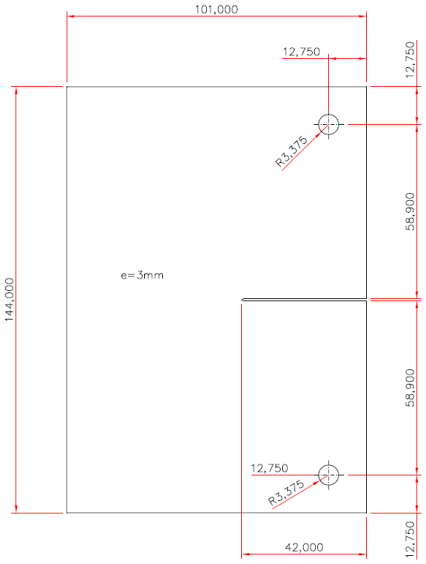

Figure 3. Measurements of specimen in mm.

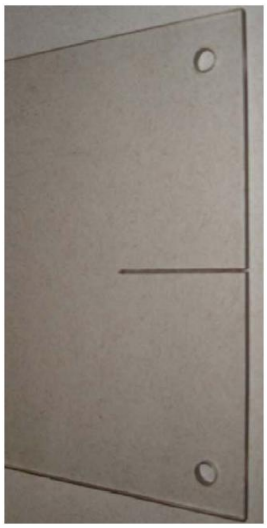

Figure 4. Photoelastic Specimen.

Figure 5. Applied load of 0N.

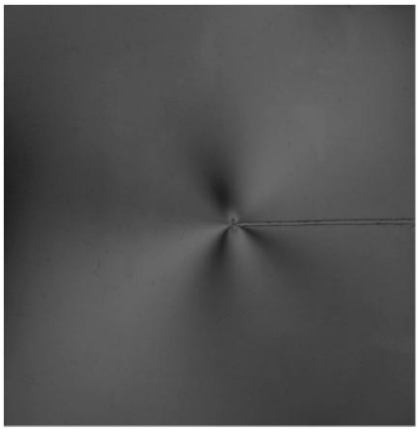

Figure 6. Applied load of 50N.

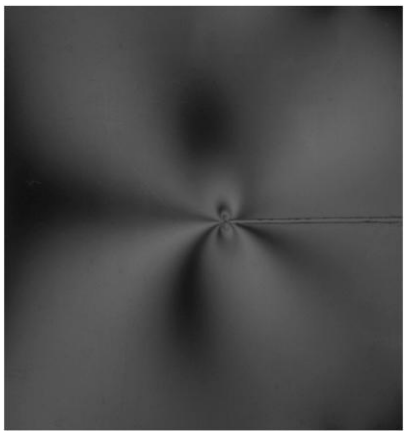

Figure 7. Applied load of 100N.

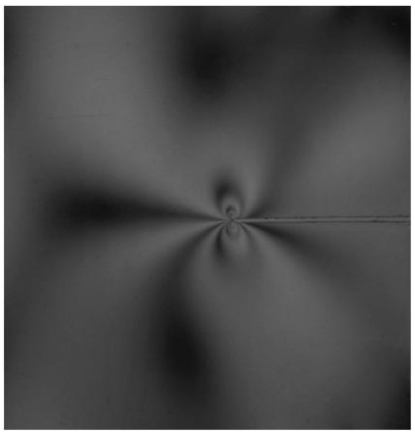

Figure 8. Applied load of 150N.

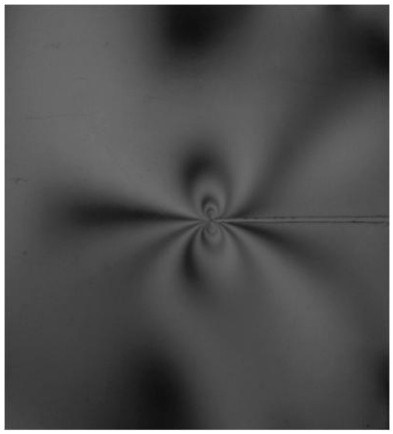

Figure 9. Applied load of 200N.

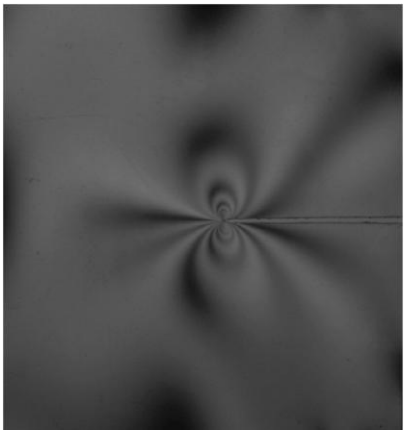

Figure 10. Applied load of 250N.

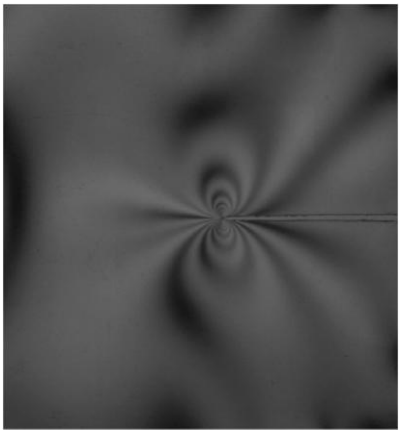

Figure 11. Applied load of 300N.

Images captured by the system, were processed using two software developed by (Soares, 1997): FOTOFRAN and FOTOVISTA. The first allows to treat images (modify contrast, brightness, apply filters, etc..) skeletonized, refining, labeling isochromatic fringes and preparing the data for calculation of the Stress Intensity Factor, which is performed by the second software. It is shown in Fig. 12 the steps developed by software FOTOFRAN.

The method of calculating stress intensity factor used was the Overdeterministic Method proposed by Dally (Soares, 1997; Dally and Riley, 2005). These calculations were performed in several load steps, starting at *P = 50N*, and from which isochromatic became clear enough to be processed by load *P = 300N*, corresponding to the end of the test.

To illustrate this process, consider fringe pattern of Fig. 10, corresponding to load *P = 250N*. This image, after filters applications to improve their quality was skeletonized by software FOTOFRAN. From this point, this software generates a file FOTOFRAN to calculate stress intensity factor value, K_I, in FOTOVISTA. Figure 13 shows functions processed using FOTOVISTA.

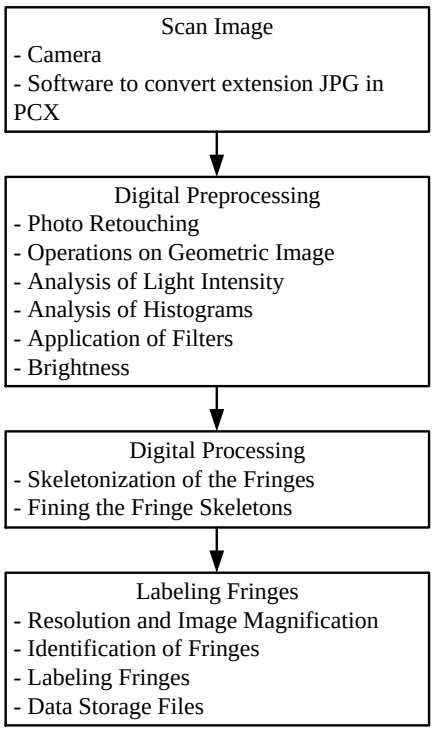

Figure 12. Steps undertaken in the software FOTOFRAN.

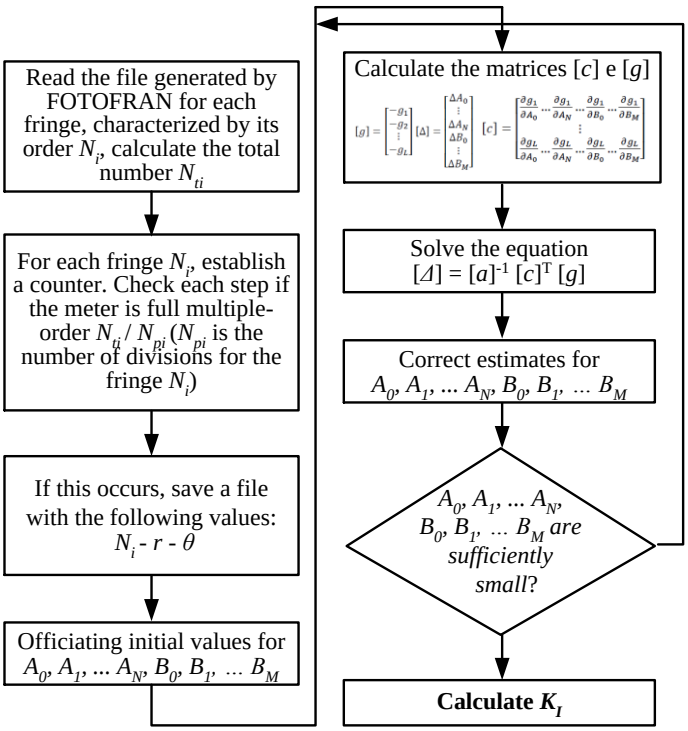

Figure 13. Steps undertaken in the software FOTOVER.

4. NUMERICAL ANALYSIS

To perform numerical analysis in order to determine stress intensity factor, numerical models were similar to those adopted in the experimental photoelastic analysis. It was adopted the same parameters of the photoelastic test.

All numerical simulation analysis were performed using finite element ANSYS® Software. It was built on a model element PLANE82 as in Fig. 3. Importantly, this element has a mobile intermediate node, which is a necessary feature for calculating stress intensity factor.

The following physical properties PSM-1 were used:

- Modulus of elasticity (E): E = 2,39 GPa for temperatures between -20 ºC and 43 ºC;
- Poisson's ratio (υ): υ = 0,383
- Density (ρ): ρ = 1170Kg/m³

After being defined all basic assumptions, as element type to be used and descriptions of physical properties of the material, a study was conducted to validate numerical analysis from Dowling (1999) quotations, which presents numerical solution for point loading given by Eq. (24):

$$K = F_p \frac{P}{t\sqrt{b}} \tag{24}$$

where P = load in the elastic; b = width; t = thickness and F_p= constant tabulated that comes from a/b.

The Ansys® software is used widely for Calculating Stress intensity factor. Some works performed by Miranda *et al.* (2003), Patrama *et al.* (2005), Phan (2006) and several other authors, used this tool for determining stress intensity

factor. Its use had good accuracy for the study conducted here, as in test case (Phan, 2006). Values obtained for this study showed a difference of 3.3% compared between numerical analysis and experimental results.

KSCON use the command to generate mesh at the crack tip, and this command was used with the following parameters:

- Radius of the first layer of elements = $1x10^{-4}$m;
- Ratio between the length of the second and the first layer of elements = 0,25;
- Number of elements around the crack tip = 11;
- Location of central nodes of singular elements: distance to the crack tip a quarter of length of the edge.

Calculation of stress intensity factor K_I was carried out by the command KCAL. It was adopted physical properties PSM-1, and the boundary conditions of the test, as loadings and restrictions. The method used by Ansys® software to determine the stress intensity factor was direct displacement extrapolation.

5. RESULTS

5.1. Experimental Analysis

It was calculated stress intensity factor K_I for various applied loads, starting at $P = 0N$ to $P = 300N$, an increment of $50N$. For each applied load, this procedure was performed six times, resulting in six values of K_I. Table 1 shows the results of this calculation and Fig. 14, a graph of values of K_I to the loading adopted.

Table 1. Results of experimental analysis of photoelastic

Load [N]	Measure 1 [$MPa.m^{1/2}$]	Measure 2 [$MPa.m^{1/2}$]	Measure 3 [$MPa.m^{1/2}$]	Measure 4 [$MPa.m^{1/2}$]	Measure 5 [$MPa.m^{1/2}$]	Measure 6 [$MPa.m^{1/2}$]	Average [$MPa.m^{1/2}$]	Standard Deviation [$MPa.m^{1/2}$]
0	0	0	0	0	0	0	0	0
50	0.212329	0.326203	0.462402	0.470455	0.18932	0.187793	0.308035	0.1213
100	0.465936	0.515887	0.594135	0.552481	0.579205	0.546453	0.542349	0.0422
150	0.855659	0.912981	0.862186	0.750758	0.901856	0.748429	0.838644	0.0661
200	1.179855	0.914606	1.152252	1.166865	1.151114	0.801970	1.061110	0.1474
250	1.382246	1.360083	1.392829	1.406468	1.340452	1.405839	1.381319	0.0241
300	1.543460	1.947239	1.933417	1.779004	1.326192	1.471922	1.666872	0.2351

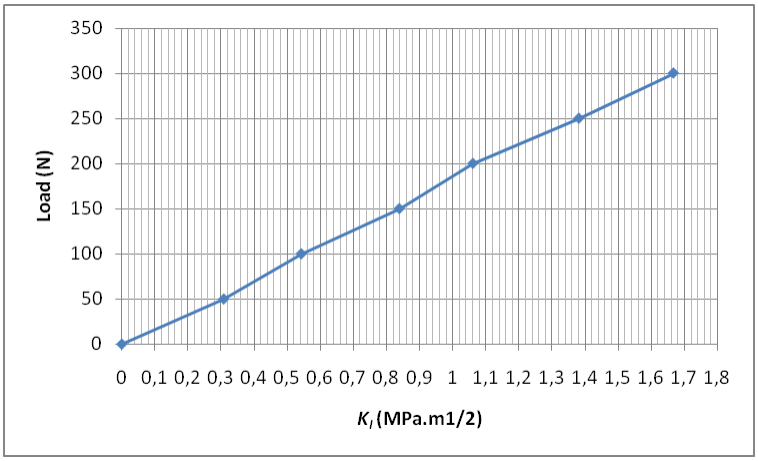

Figure 14. Graph of test results with experimental photoelastic technique: Load x K_I.

5.2. Numerical Analysis

Numerical analysis by finite element method obtained values of Stress intensity factor K_I, for the same loads that were made in photoelastic analysis. Figures 15 to 20 show the distribution of difference between principal stresses (σ_1-σ_2). For these stress differences, there is a need to make a calibration range of results.

Table 2 shows results of calculation of K_I and Fig. 21, a graph of values of K_I in relation to loads used.

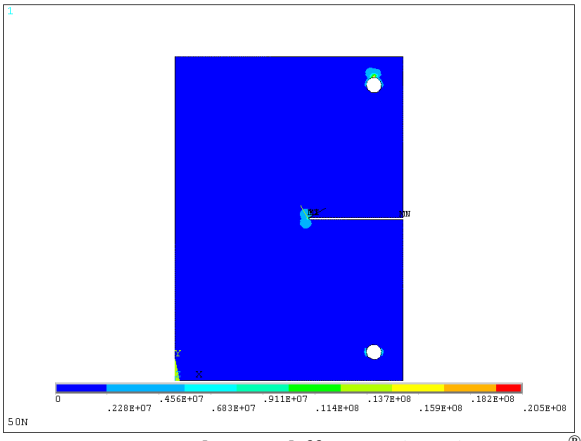

Figure 15. Principal stress difference (σ_1-σ_2) in Ansys®, for *P=50N*.

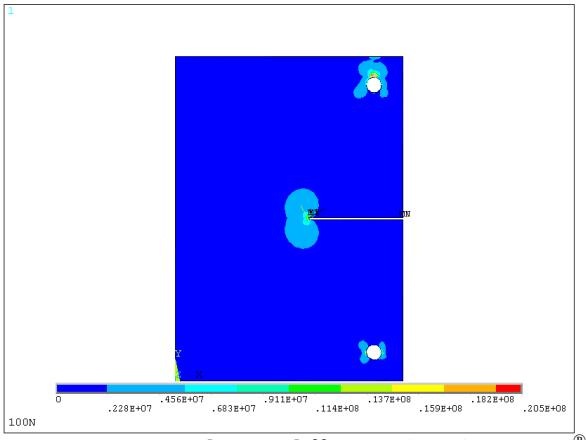

Figure 16. Principal stress difference (σ_1-σ_2) in Ansys®, for *P=100N*.

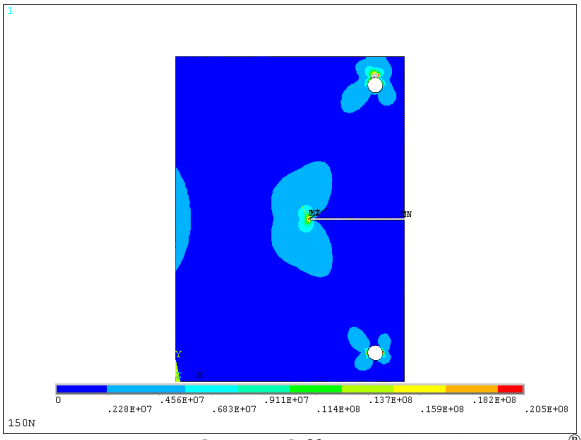

Figure 17. Principal stress difference (σ_1-σ_2) in Ansys®, for *P=150N*.

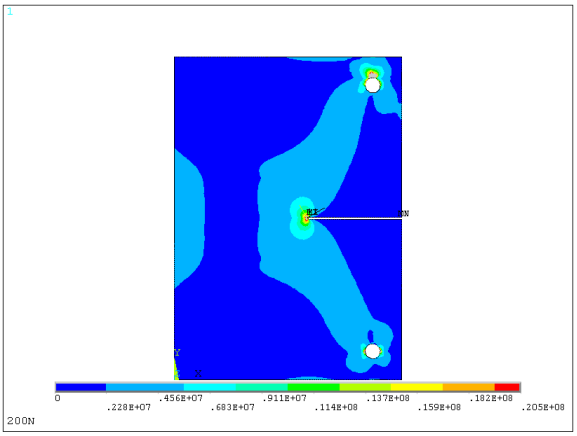

Figure 18. Principal stress difference (σ_1-σ_2) in Ansys®, for *P=200N*.

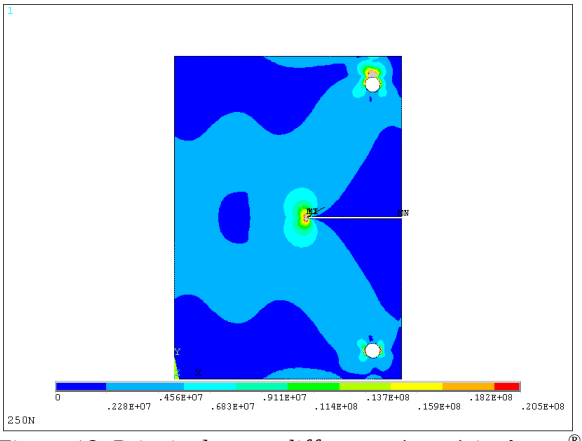

Figure 19. Principal stress difference (σ_1-σ_2) in Ansys®, for *P=250N*.

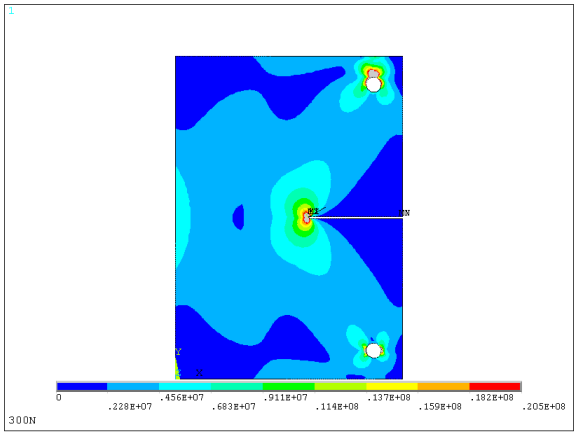

Figure 20. Principal stress difference (σ_1-σ_2) in Ansys®, for *P=300N*.

Table 2. Results of numerical analysis by finite element method

Load [*N*]	Measure [$MPa.m^{1/2}$]
0	0
50	0.27179
100	0.54358
150	0.81538
200	1.08720
250	1.35900
300	1.63080

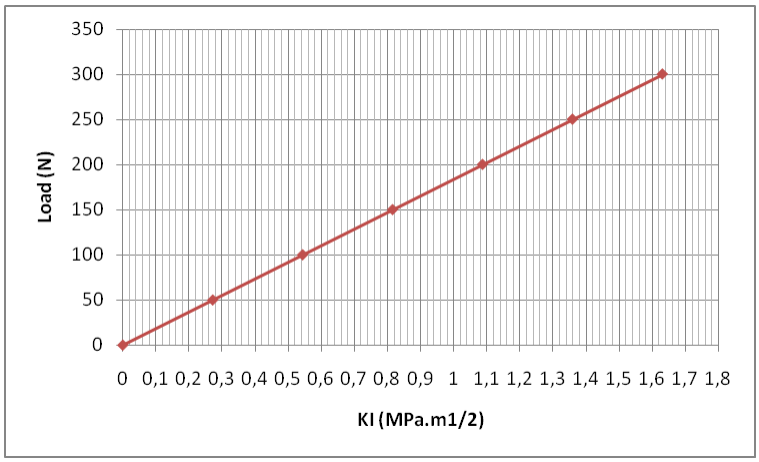

Figure 21. Graph of numerical analysis results by finite element method: Load x K_I.

5.3. Comparison of Results

Table 3 shows the comparison of results for values of stress intensity factor K_I and yet difference in results.

Table 3. Comparison of results for the values of stress intensity factor K_I

Load [N]	Measure - FOTOVER [$MPa.m^{1/2}$]	Measure - ANSYS® [$MPa.m^{1/2}$]	Difference [%] FOTOVER / ANSYS®
0	0	0	0.000 %
50	0.308035	0.27179	11.767 %
100	0.542349	0.54358	-0.227 %
150	0.838644	0.81538	2.774 %
200	1.061110	1.08720	-2.459 %
250	1.381319	1.35900	1.616 %
300	1.666872	1.63080	2.164 %

An important consideration to be made is that, since the studies by using photoelasticity models are developed, it is necessary that results could be extrapolated to prototype. Relationship between model and prototype was established using model theory and dimensional analysis, as described by Carneiro (1996).

Compared results obtained by experimental analysis and numerical analysis, are shown in Fig. 22.

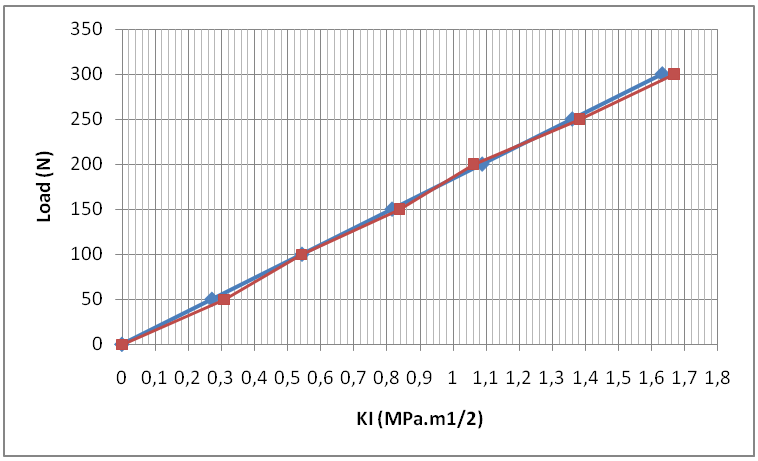

Figure 22. Graph comparing experimental and numerical analysis results: Load x K_I.

6. CONCLUSIONS

The methodology used in this analysis presented an alternative photoelastic experimental method valid and reliable for determining stress intensity factor K_I caused by static loading. Preparation of specimens used in the test were relatively simple but requires some care in specimen preparation, so as not to cause stress concentrations in machining, as this could cause interference in the results. The greater difference experimental and numerical analysis results was found to be of 11.70%, and obtained an average difference of at most ± 3%, where these values are within satisfactory limits. It is emphasized that one should take care with a very low load values, because sampling of fringes are very small, as seen in the results as obtained for the loading of 50N, which explains one of the possibilities for the large difference obtained in this loading. For applied load of 300N, one must be very careful for avoiding a possible lateral buckling, although it was not perceived in this test.

7. REFERENCES

Ayatollahi, M. R. and Nejati, M., 2010, "An over-deterministic method for calculation of coefficients of crack tip asymptotic field from finite element analysis". Fatigue & Fracture of Engineering Materials & Structures, Volume 34, March 2010, Pages 159–176. DOI: 10.1111/j.1460-2695.2010.01504.

Carneiro, Fernando L., 1996, "Análise Dimensional e Teoria da Semelhança e dos Modelos Físicos", 2.Ed. Rio de Janeiro: UFRJ EDITORA.

Dally, J. W., and Riley, W. F., 2005, "Experimental Stress Analysis", 4th ed., College House Enterprises, Knoxville, TN.

Dowling, Norman E., 1999, "Mechanical Behavior of Material, Engineering Methods for Deformation, Fracture, and Fatigue", 1.Ed. New Jersey: PRENTICE HALL.

Irwin, G.R.; De Wit, R., 1983, "A Summary of Fracture Mechanics Concepts". Journal of Testing And Evaluation, New York, vol.11, issue 1.

Miranda, Antônio C.O. et al., 2003, "Finite Element Modeling of Fatigue Crack Bifurcation". Journal Computational Fluid and Solid Mechanics, Rio de Janeiro.

Quinan, Marco A.D., 2005, "Uma Metodologia para Determinação do Fator de Intensidade de Tensões Causado por Tensões Térmicas Utilizando Fotoelasticidade". TESE (DOUTORADO) - Instituto de Pesquisas Energéticas e Nucleares (USP), São Paulo.

Patrama, Stefan D.; ILIESCU, Nicole; ATANASIU, Costica, 2005, "Photoelastic Analisis for Overdeterministic Calculation of the Stress Intensity Factor". Journal Experimental Methods e Solid Mechanics, Parma (22º Danubia-Adria Symposito).

Phan, A.V. ANSYS Tutorial, 2006, "*2D Fracture Analysis"*, ANSYS Release 7.0, University of South Alabama.

Post, Dan, 1954, "Photoelastic Stress Analysis for an Edge Crack in a Tensile Field" in: Spring Meeting of the Society for Experimental Stress Analysis, Cincinnati.

Soares, Wellington A., 1997, "Determinação de Parâmetros da Mecânica de Fratura a Partir se Imagens Fotoelásticas – Usando Processamento Digital". TESE (DOUTORADO) - Instituto de Pesquisas Energéticas e Nucleares (USP), São Paulo.

8. RESPONSIBILITY NOTICE

The authors are the only responsible for the printed material included in this paper.